

Atomistic modeling of uranium monocarbide with a machine learning interatomic potential

Lorena Alzate-Vargas,¹ Kashi N. Subedi,¹ Roxanne M. Tutchton,¹
Michael W.D. Cooper,² Tammie Gibson,¹ and Richard A. Messerly^{1,3}

¹*Theoretical Division, Los Alamos National Laboratory,
Los Alamos, New Mexico 87545, USA*

²*Materials Science and Technology Division,
Los Alamos National Laboratory, Los Alamos, New Mexico 87545, USA*

³*National Center for Computational Sciences Division,
Oak Ridge National Laboratory, Oak Ridge, TN 37830, USA*

Abstract

Uranium monocarbide (UC) is an advanced ceramic fuel candidate due to its superior uranium density and thermal conductivity compared to traditional fuels. To accurately model UC at reactor operating conditions, we developed a machine learning interatomic potential (MLIP) using an active learning procedure to generate a comprehensive training dataset capturing diverse atomic configurations. The resulting MLIP predicts structural, elastic, thermophysical properties, defect formation energies, and diffusion behaviors, aligning well with experimental and theoretical benchmarks. This work significantly advances computational methods to explore UC, enabling efficient large-scale and long-time molecular dynamics simulations essential for reactor fuel qualification.

I. INTRODUCTION

Uranium monocarbide (UC) is an advanced ceramic fuel considered promising for use in Generation-IV nuclear reactor systems, such as gas-cooled and sodium-cooled fast reactors, due to its favorable nuclear and thermal properties [1, 2]. Specifically, UC possesses a significantly higher uranium density and superior thermal conductivity compared to conventional oxide-based fuels like uranium dioxide (UO_2), making it attractive from both an economic and a safety perspective [3–5]. However, these advantageous properties are accompanied by critical challenges, including pronounced fuel swelling and substantial fission gas release under operational conditions, complicating its practical deployment.

To overcome these challenges and evaluate the viability of UC as a nuclear fuel, a robust understanding of the underlying structure-property relationship is essential. However, experimental research on nuclear fuel materials presents many difficulties as it requires processing and measuring radioactive samples. Atomistic modeling methods, particularly density functional theory (DFT), have proven to be effective in studying fundamental properties of UC such as point defect formation, diffusion mechanisms, and incorporation of fission products within nuclear fuels [6–9]. Previous work [6] reported point defect formation energies and provided valuable insights into the accommodation of helium, xenon, and oxygen impurities. Later work [7] further investigated defect migration mechanisms, revealing that uranium and carbon vacancies play a dominant role in atomic diffusion processes. Additional studies [8, 9] expanded on these results by analyzing the incorporation energies and diffusion behaviors of fission products, highlighting the efficacy of DFT in capturing fundamental defect phe-

nomena.

However, DFT has notable limitations when applied to strongly correlated materials such as UC, particularly due to difficulties in accurately representing the localized nature of the uranium $5f$ electrons. To better account for electron-electron interactions in strongly correlated electron systems, one can improve the Coulomb interaction term in DFT calculations by adding the the Hubbard (U) parameter. DFT+ U markedly improves the prediction of elastic constants, and electronic structure of UC [10]. Similarly, it gives accurate lattice dynamics, phonon dispersions, and overall thermodynamic stability [11] compared to DFT, bringing the computational results closer in alignment with the experimental observations.

More recent work [12] specifically utilized DFT+ U calculations to study intrinsic defects and xenon impurities, providing detailed energetic insights essential for understanding irradiation behavior. These findings underscore that the Hubbard term provides more reliable data on defect energetics and diffusion barriers, crucial parameters for accurately modeling UC under reactor operating conditions.

Although computing certain single-point properties with DFT+ U is relatively straightforward, predicting structural and thermophysical properties requires long-time averaging of molecular dynamics (MD) simulations. Despite advancements in electronic structure methods and computing hardware, performing long MD simulations with DFT+ U remains extremely computationally expensive. Classical potentials provide a more practical route from a computational standpoint, however existing classical potentials exhibit only moderate accuracy in reproducing experimental and theoretical results for structural and thermophysical properties [13, 14]. Therefore, there is a clear need for computationally efficient yet highly accurate approaches to effectively model UC at large scales and extended timescales relevant to reactor conditions.

Machine learning interatomic potentials (MLIPs) offer a promising solution to bridge this gap, combining near-DFT+ U accuracy with computational efficiencies that remain comparable to classical potentials. Recent implementations of MLIPs have shown remarkable success in accurately modeling uranium-based materials, including elemental uranium [15], uranium dioxide (UO_2) [16, 17] and uranium mononitride (UN) [18], across a wide range of thermophysical conditions and defect configurations. These studies have demonstrated the importance of active learning for generating a diverse and representative training dataset. A properly trained MLIP enables detailed exploration of nuclear fuels under realistic operating

conditions.

In this work, we present the first MLIP specifically developed for uranium monocarbide, based on the Hierarchically Interacting Particle Neural Network (HIP-NN) architecture [19, 20]. We utilize an active learning framework guided by uncertainty quantification and MD sampling to generate a DFT+ U quality training dataset for UC, which includes various defect structures relevant to nuclear applications of UC. We subsequently validate our MLIP by predicting fundamental thermophysical properties, elastic constants, defect energies, migration and self-diffusion activation energies, comparing these predictions against experimental data and DFT/DFT+ U calculations. In the absence of reliable classical potentials or experimental data, our MLIP provides predictions for properties that were previously unattainable with DFT+ U . Our results demonstrate that the developed MLIP reliably captures critical features of UC, significantly advancing our ability to perform comprehensive and accurate atomistic simulations of this advanced nuclear fuel.

II. METHODS

A. Density functional theory calculations

All density functional theory (DFT) calculations performed in this study used the frozen-core, all-electron projector-augmented-wave (PAW) method [21], implemented in the Vienna *ab initio* simulation package (VASP) [22, 23]. We used the generalized gradient approximation (GGA) as parametrized by Perdew, Burke, and Ernzerhof (PBE) [24] as the exchange-correlation functional. A plane-wave basis set with a cutoff energy of 520 eV was used, along with the Methfessel-Paxton smearing scheme (smearing width of 0.1 eV) for electronic occupancies. The energy and force convergence criteria were set as 10^{-8} eV and 10^{-4} eV/Å, respectively.

To accurately describe the strongly correlated nature of uranium $5f$ electrons, we incorporated the DFT+ U approach developed by Dudarev et al. [25]. Within this method, only the effective Hubbard parameter ($U_{\text{eff}} = U - J$), representing the difference between the Hubbard parameter U and the exchange parameter J , is explicitly defined.

We carried out a systematic investigation to determine the optimal value of U_{eff} , exploring both non-magnetic (NM) and type-I antiferromagnetic (AFM-I) orderings in a NaCl-type

structure. The AFM ordering was modeled by assigning alternating magnetic moments to uranium atoms in consecutive (001) planes, resulting in a net zero magnetic moment, as depicted in Fig. 1. We performed calculations for various U_{eff} values, keeping the exchange parameter fixed at $J = 0.5$ eV. For each value of U_{eff} , the lattice parameter, elastic constants, and phonon dispersions were computed and compared against experimental data.

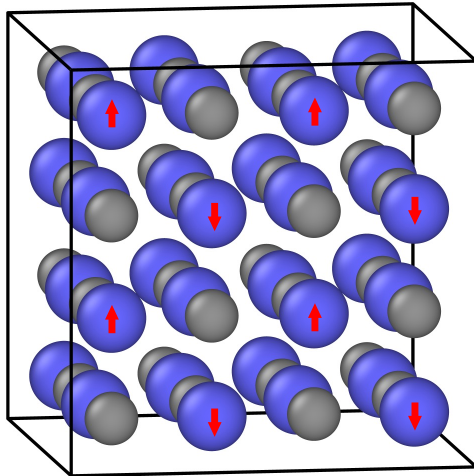


Figure 1: Perspective view of the UC crystal structure in the AFM-I phase and magnetic moments for uranium along the (001) direction (red arrows). The U atoms and C atoms are represented by blue and gray spheres, respectively.

Unit cell calculations of lattice parameter and elastic constants were performed using a dense $12 \times 12 \times 12$ Monkhorst-Pack k -point mesh with Brillouin zone integration. The input files required for elastic constant calculations were generated using VASPKIT [26]. Phonon dispersion curves were calculated with the PHONOPY code [27], utilizing the finite displacement method with atomic displacements set at 0.015 \AA . Phonon calculations used a $2 \times 2 \times 2$ supercell containing 64 atoms and a $4 \times 4 \times 4$ k -point mesh.

The computed lattice constants, bulk moduli, and elastic constants for different U_{eff} values and magnetic configurations are summarized in Table I. We also included the corresponding values when using DFT on both configurations and SCAN on the NM ordering, where we can see a large deviation in the prediction of C_{11} and C_{44} . However, when comparing the DFT+ U predictions, no single choice of U_{eff} simultaneously reproduces all experimental properties perfectly. Generally, NM ordering calculations tend to overestimate the elastic constant C_{12} and bulk modulus despite reasonable predictions of the lattice parameter. Conversely,

AFM ordering systems with U_{eff} values of 1.25 and 1.35 eV exhibit improved consistency with experimental data. Among these, $U_{\text{eff}} = 1.25$ eV provides the closest agreement with experimental phonon dispersions (shown in Fig. 2) and bulk moduli. Consequently, we selected a U_{eff} value of 1.25 eV in the AFM-I configuration for performing all reference DFT+ U calculations in this study.

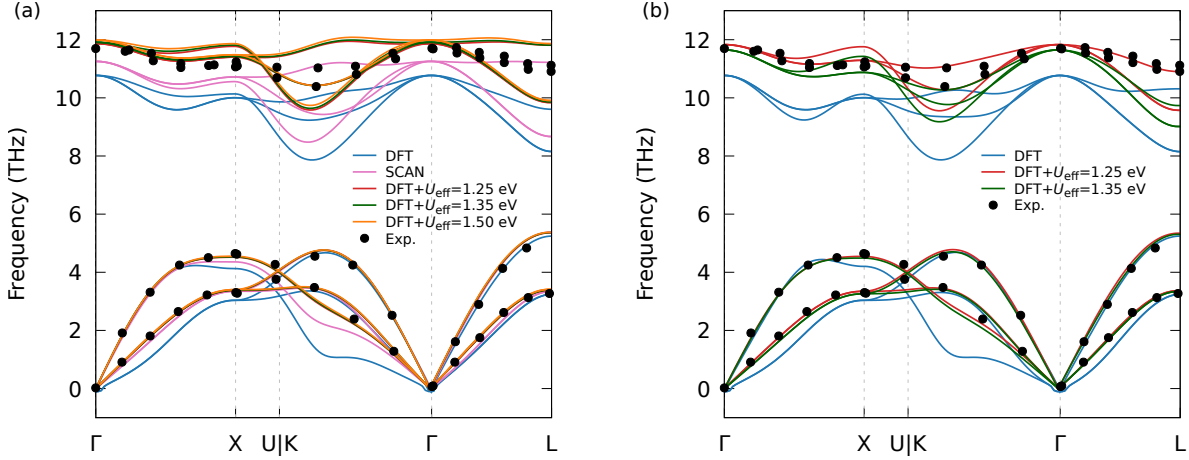


Figure 2: Phonon band structures for (a) NM ordering and (b) AFM ordering using DFT, SCAN and DFT+ U with different U_{eff} values. Experimental data from Ref. [28] included as black points. AFM structure with $U_{\text{eff}}=1.25$ eV calculations capture experimental optical modes better than the other values.

B. Active learning procedure for dataset generation

An accurate MLIP depends on the diversity and representativeness of its training dataset. To systematically and efficiently construct such, we employed an active learning (AL) methodology proposed in Ref. [32, 33]. The AL procedure aims to identify high-uncertainty atomic configurations by quantifying the variance in predicted energies and forces across an ensemble of eight semi-independent MLIPs. Each MLIP in the ensemble was trained on distinct random splits of training, validation, and test datasets and initialized with different model parameters. Configurations with high variance (high uncertainty) among the ensemble predictions were selected for inclusion in subsequent iterations of training, enhancing model accuracy and robustness. New candidate structures were sampled using MD simulations driven by an individual member of the ensemble of MLIPs. To facilitate rapid exploration

Table I: Equilibrium properties of UC, including lattice parameter, bulk modulus, and elastic constants calculated using different U_{eff} values for DFT+ U at 0 K and comparing NM and AFM magnetic orderings.

Functional	Ordering	Lattice parameter (Å)	B (GPa)	C_{11} (GPa)	C_{12} (GPa)	C_{44} (GPa)
DFT	NM	4.933	187.1	290.5	135.3	24.7
DFT	AFM	4.933	186.7	291.5	134.4	24.7
SCAN	NM	4.938	181.7	290.7	132.0	33.3
DFT+ U (U_{eff} =1.25 eV)	NM	4.950	191.5	304.8	134.8	43.2
DFT+ U (U_{eff} =1.25 eV)	AFM	4.953	159.4	332.7	72.8	47.9
DFT+ U (U_{eff} =1.35 eV)	NM	4.951	192.1	306.3	135.0	44.7
DFT+ U (U_{eff} =1.35 eV)	AFM	4.957	151.4	318.5	67.9	50.4
DFT+ U (U_{eff} =1.50 eV)	NM	4.953	192.8	308.4	135.0	47.0
Exp. at 300 K (Refs. [29–31])	-	4.956	156–158	314–320	77–79	64–66

of the potential energy surface, the temperature and density were dynamically modulated during each MD simulation through combined linear and sinusoidal adjustments, following work done in Ref. [33]. Temperatures were varied from an initial temperature between 1000–5000 K to a final temperature between 100–5000 K, while densities were selected between 10 and 17 g/cm³. Density variations were implemented by scaling both the atomic positions and simulation cell dimensions accordingly, allowing the system to explore configurations representative of realistic operational scenarios and defect states.

The AL loop was initiated from a bootstrap dataset consisting of 200 configurations which were carefully selected from a subset of the training dataset developed for uranium nitride MLIP, using a similar AL approach [18]. In this work, each N atom was substituted with a C atom. The bootstrap dataset includes face-centered cubic NaCl-type structures, high-temperature systems, and various defect configurations (e.g., Frenkel pairs and C/U bivacancies). Given the small difference between the lattice parameters of UC (recommended value of 4.96 Å [31], as value varies from 4.91–4.99 Å [5] depending on carbon content,) and UN (4.88 Å), we rescaled the atomic positions and simulation boxes for the initial

configurations by approximately 1.4% to better represent the equilibrium U-C bond lengths.

Single-point DFT+ U calculations were performed to compute energies and atomic forces for each configuration selected by AL. To trade off computational cost and efficiency, a k -point mesh of $2 \times 2 \times 2$ was adopted. The final training dataset consisted of 6,743 configurations of $2 \times 2 \times 2$ supercells containing approximately 64 atoms, with slight variations due to defect formation, providing diverse structures and comprehensive coverage of relevant atomic environments required for a robust and reliable MLIP.

C. Machine learning potential

HIP-NN is a message-passing neural network where the characterization of the environment takes place through learned parameters using sensitivity functions which characterize distances between atoms, and interaction functions which combine the distances and weights of neighboring atoms to form a message. HIP-NN was successfully implemented to model uranium nitride over a wide temperature range [18]. Therefore, we used the same network parameters selected for UN, i.e, one interaction layer ($n_{\text{interaction}} = 1$), $n_{\text{feature}} = 60$ neurons per layer and $n_{\nu} = 20$ sensitivity functions. Similarly, the interaction form was improved by using the HIP-NN with tensor [20] of order $\ell = 1$, that is, vector-based message passing, which improves over the original HIP-NN by summing messages generated from neighbors not only as scalars, but also as vectors, which allows individual neurons to be sensitive to angles between neighbors. The training of the MLIP was done using the open-source implementation of HIP-NN *hippynn* [34].

D. Molecular dynamics simulations

MD simulations to validate and evaluate the performance of the developed MLIP were performed using the Large-scale Atomic/Molecular Massively Parallel Simulator (LAMMPS) software package [35], which directly interfaces with the HIP-NN architecture.

To characterize the mechanical response of uranium monocarbide at zero Kelvin, we computed the elastic constants using the deformation method. These calculations were carried out using a $5 \times 5 \times 5$ supercell of the rock-salt crystal structure at 0 K. The same system size was used to determine defect formation energies and to compute the activation energies

of point defect migration by using the nudged elastic band (NEB) method implemented in LAMMPS.

Temperature-dependent lattice parameters were obtained from a series of isobaric-isothermal (NPT) simulations performed on the MLIP ensemble. We used a $15 \times 15 \times 15$ supercell and covered a temperature range from 300 K up to 2500 K. The Nosé–Hoover thermostat and barostat were utilized to maintain the target temperature and zero pressure, respectively. Thermostat and barostat damping parameters were set to 1 ps and 0.5 ps, with simulations running for a total duration of 30 ps using a timestep of 1 fs. Equilibrium lattice parameters were calculated by averaging simulation box dimensions over the final 10 ps of each simulation to ensure convergence and accurate thermodynamic averaging.

Self-diffusion coefficients for carbon and uranium atoms under the presence of defects were calculated by extracting the mean square displacements from NVE simulations held for 1 ns at a specific temperature in the range of 1800 K to 2300 K. These simulations were performed on $15 \times 15 \times 15$ supercell systems with varying stoichiometric conditions.

III. RESULTS

To demonstrate the robust predictive capability of the HIP-NN potential developed for UC, we evaluate some relevant thermophysical and transport properties and compare them with available experimental data.

The final MLIP trained on our dataset achieves a total energy root mean square error (RMSE) of 15.9 meV/atom and a force RMSE of 0.55 eV/Å. These values compare favorably—though they are somewhat higher—than those reported for a previously developed HIP-NN MLIP for UN trained on DFT data [18], which achieved energy and force RMSEs of 2.48 meV/atom and 0.113 eV/Å, respectively.

A first validation of the MLIP is given in Table II, where we present the calculated values of lattice parameter a at 300 K, elastic constants at 0 K, and bulk modulus at 0 K. We compare the MLIP predictions with reference experimental data and values obtained by Chartier and Brutzel [14] using their empirical potential. The calculated DFT+ U values from this work are also added. While we find that the MLIP predicts a lower value of C_{11} in comparison to the DFT+ U data, while achieving higher accuracy for the values of C_{12} and C_{44} . The resulting bulk modulus at zero temperature shows excellent agreement

with the experimental data.

Table II: Comparison of lattice parameter (a) at 300 K, elastic constants at 0 K and bulk modulus at zero pressure and 0 K (B_0) for UC obtained from the MLIP, an empirical potential, DFT+ U calculations, and experimental data.

	a 300 K	C_{11}	C_{12}	C_{44}	B_0
	(Å)	(GPa)	(GPa)	(GPa)	(GPa)
HIP-NN	4.98	290	79	57	150
Classical potential (Ref. [14])	4.96	322	104	39	176
DFT+ U (This work)	4.95	333	73	48	160
Exp. at 300 K (Refs. [29–31])	4.956	314–320	77–79	64–66	156–158

To confirm the MLIP ability to simulate stoichiometric UC in the FCC NaCl-type structure; we calculate the lattice parameter at zero pressure as a function of temperature as shown in Fig. 3. The MLIP is capable of performing stable MD simulations up to 2500 K, below melting temperature of 2780 K for UC_{~1.0} [36]. It should be noted that the melting point of UC is highly dependent on the carbon content and many of the uranium monocarbide high-temperature properties, including the lattice parameter, homogeneously extend up to the β -UC₂ composition.

For comparison, Fig. 3 includes the lattice parameter obtained from DFT-MD simulations performed with the reference DFT+ U where $U_{\text{eff}}=1.25$ eV, used in the training. Our MLIP lattice parameter is in excellent agreement with the predicted DFT-MD lattice parameter over the temperature range studied. However, it is known that DFT+ U often overestimates the lattice parameter for strongly correlated systems. Consequently, we find that at temperatures below 1500 K, the MLIP also overestimates the lattice parameter compared to the experimental data. This appears to be minimized as the temperature increases, where the MLIP matches the experiments.

Point defects and diffusion

Radiation damage in reactor conditions produces point defects and fission products, both of which significantly impact the service performance of nuclear fuels. Point defects such as

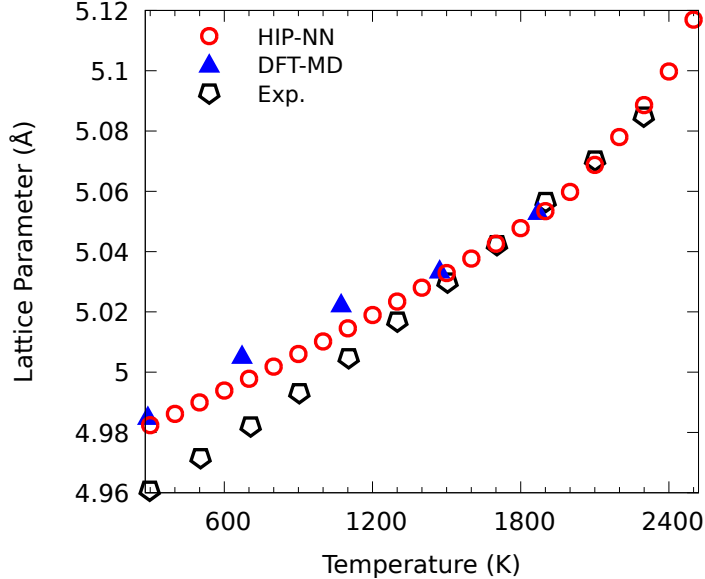


Figure 3: Comparison of lattice parameter as a function of temperature obtained from MLIP, DFT+ U -MD, and experimental data from Ref. [37].

vacancies serve as trapping sites for impurities and are critical to diffusion-driven processes. To evaluate the performance of our MLIP and understand the role of defects in uranium carbide, we report the formation energies of neutral point defects—including uranium and carbon Frenkel pairs and Schottky defects—in Table III. While the MLIP tends to overestimate formation energies relative to DFT and experiment, the overall trends are consistent. For instance, the MLIP predicts a formation energy of 5.2 eV for the carbon Frenkel pair, overestimating the experimental value of 2.2 eV [38]. It is important to interpret these comparisons with caution, as experimental measurements often involve samples with oxygen and nitrogen impurities and may not reflect perfectly. Yet the carbon FP value improves with the only available empirical potential tailored to model diffusion in UC.

The migration barriers of uranium and carbon vacancies (vac) and interstitials (int) are presented in Table IV. We report values predicted by our MLIP, alongside data from an empirical potential, DFT, DFT+ U calculations available in the literature, and experimental measurements, extracted from electrical resistivity measurements of quenched UC samples, were reported by Schüle and Spindler [39] and later by Matsui and Matzke [40]. These measurements used samples intended to be stoichiometric UC, although all specimens contained measurable oxygen and nitrogen impurities.

Table III: Comparison of neutral point defect formation energies for uranium Frenkel pair (FP_U), carbon Frenkel pair (FP_C), and Schottky defects (SD) obtained from MLIP, an empirical potential, DFT calculations, and experiments.

	FP_U	FP_C	SD
	(eV)	(eV)	(eV)
HIP-NN	10.8	5.2	7.2
Classical potential (Ref. [14])	6.8	1.5	-
DFT (Ref. [7])	7.6	3.4	4.3
DFT+ U (This work)	8.1	3.4	3.8
Experiment (Ref. [38])	-	2.2	-

Our MLIP predicts the same migration energy (3.0 eV) for both carbon and uranium vacancies. This contrasts with experimental data and DFT and DFT+ U calculations, which consistently report different migration energies between carbon and uranium. Schüle and Spindler reported experimental activation energies of 1.45 eV for carbon vacancy migration and 2.2 eV for uranium. Matsui and Matzke found even lower values—0.9 eV for carbon and 2.4 eV for uranium—emphasizing the variability introduced by microstructural and chemical impurities. The migration energy for an uranium interstitial predicted by the MLIP is 1.02 eV, showing an excellent agreement with respect to DFT+ U calculations.

Despite the MLIP overestimating activation energies of vacancies, it correctly captures relative trends found in DFT calculations—such as the lower barrier for interstitial diffusion versus vacancy diffusion. Future refinements could improve the quantitative accuracy by including NEB-like configurations in the training dataset.

We further extend the prediction of diffusion mechanisms by computing the activation energies from Arrhenius fits to the MD diffusion data and explore relevant experimental data. One should note that direct comparison between MLIP predictions and experiments remains challenging, specially at high temperatures, where MD simulations can reach diffusive regime, since UC could exist as a two-phase material (e.g., $\text{U} + \text{UC}$ or $\text{UC} + \text{UC}_2$), affecting the measured transport properties. Consequently, experimental activation energies from self-diffusion vary widely—from 1.9 to 4.1 eV for carbon [41–44], and from 3.6

Table IV: Activation energy for migration of uranium and carbon vacancies (vac) and interstitials (int) extracted from NEB calculations using the MLIP and compared to an empirical potential, DFT and DFT+ U NEB calculations, and experimental data.

	C_{vac}	U_{vac}	C_{int}	U_{int}
	(eV)	(eV)	(eV)	(eV)
HIP-NN	3.0	3.0	-	1.02
Classical potential (Ref. [14])	4.8	2.2	1.8	0.9
DFT (Ref. [7])	2.0	1.8	1.6	3.0
DFT+ U (Ref. [12])	2.5	1.9	0.98	1.09
Exp. (Schüle and Spindler [39])	1.45	2.2	-	-
Exp. (Matsui and Matzke [40])	0.9	2.4	-	-

to 5.4 eV for uranium [39, 45], strongly depending on composition (carbon content) and microstructure. Our MLIP predicts that uranium diffuses significantly more slowly than carbon. This trend is consistent with experiments, which report that carbon diffusion in UC is approximately 10^2 – 10^3 times faster than uranium diffusion [39, 45]. As a result, uranium diffusion in pure UC is not accessible within the time scales of our MD simulations. Instead, we report uranium diffusion for systems containing uranium defects, where the mobility is sufficiently enhanced to be captured.

Figure 4a presents the self-diffusion coefficients of carbon in UC as a function of inverse temperature for three systems: a defect-free (stoichiometric) lattice, a carbon-deficient system with 1.0% vacancies, and a carbon-rich system with 1.0% interstitials.

In the stoichiometric case, the MLIP predicts an activation energy of 4.0 eV, substantially higher than experimental values. For instance, Lee and Barrett [42] reported an activation energy of 2.7 eV between 1539–1957 K, while Makino et al. [44] found a value of 2.3 eV between 1600–2200 K. These discrepancies likely stem from the idealized nature of the simulations: the absence of native or thermally activated defects in the pristine simulation cell inhibits diffusion, leading to artificially high barriers. The presence of carbon vacancies lowers the activation energy to 3.2 eV, while interstitials reduce it further to 2.3 eV. This trend aligns with experimental observations that carbon diffusivity in UC is highly

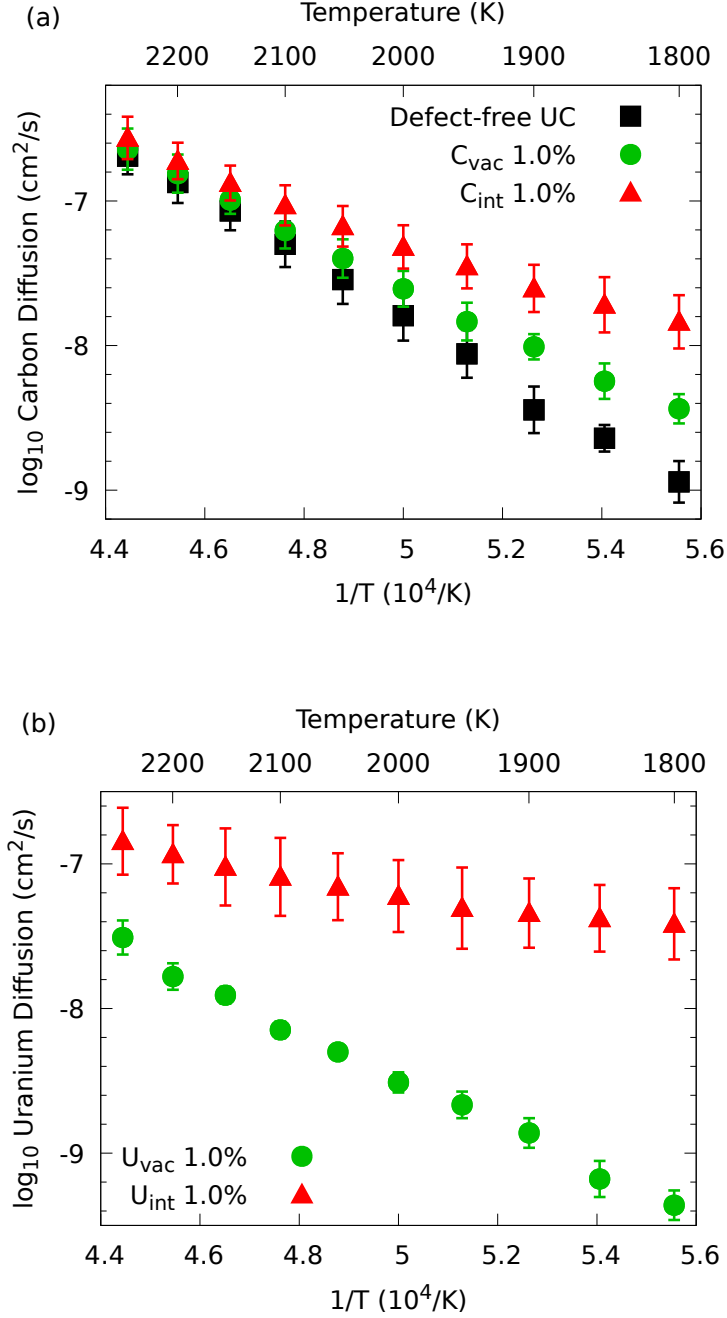


Figure 4: Self-diffusion coefficients as a function of temperature for (a) carbon in defect-free UC, carbon-deficient sample (C_{vac}), and a carbon-rich sample (C_{int}), and (b) uranium in an uranium-deficient system (U_{vac}) and an uranium-rich (U_{int}).

composition-dependent. The simulation results suggest that interstitial-mediated diffusion is the dominant path for carbon mobility under carbon-rich conditions in correlation with experimental findings.

The summary of carbon activation energies shown in Table V, demonstrates that the MLIP accurately captures the relative trends in activation energy and the effect of stoichiometry, even if the absolute barriers for vacancy diffusion remain slightly overestimated.

Table V: Comparison of MLIP-predicted activation energies (E_a) with experimental data for carbon diffusion in UC across different compositions.

Defect	MLIP E_a (eV)	Exp. Composition	Exp. E_a (eV)	Exp. T (K)	Refs.
Pure UC (defect-free)	4.0	Stoichiometric	2.3–2.7	1500–2300	[42, 44]
C vacancy	3.2	Carbon-deficient	2.7–3.9	1300–2100	[41–43]
C interstitial	2.3	Carbon-rich	1.8–2.3	1470–2300	[42, 44]

Figure 4b shows the self-diffusion coefficients of uranium in UC for systems containing either uranium vacancies or interstitials. Under stoichiometric or uranium-deficient conditions, diffusion is sluggish unless facilitated by vacancies, for which the MLIP predicts an activation energy of 3.1 eV for uranium diffusion. When uranium interstitials are introduced –uranium-rich (C-deficient) compositions–the predicted activation energy drops significantly to 1.0 eV, closely matching the NEB-calculated migration barrier of 1.02 eV, further validating the MLIP’s ability to capture defect-driven transport trends.

IV. CONCLUSIONS

We present the first MLIP specifically developed for uranium monocarbide, trained on high-quality DFT+ U data and validated across critical material properties. The MLIP demonstrates robust predictive capabilities, accurately reproducing lattice parameters, elastic constants, defect energetics, and diffusion mechanisms across a range of thermodynamic conditions. While some activation energies for defect diffusion are moderately overestimated, relative trends remain consistent with experimental observations, particularly emphasizing the importance of defect-driven transport. This MLIP represents a significant step toward improving realistic atomistic simulations that can lead to a better understanding of UC in reactor conditions and its further qualification as a fuel.

ACKNOWLEDGMENTS

The authors are grateful for insightful discussions with Benjamin Nebgen and Nicholas Lubbers regarding active learning and machine learning potentials. Los Alamos National Laboratory (LANL), an affirmative action/equal opportunity employer, is operated by Triad National Security LLC, for the National Nuclear Security Administration of the U.S. Department of Energy under Contract No. 89233218CNA000001. The research presented in this work was supported by the Laboratory Directed Research and Development (LDRD) program via project 20220053DR at LANL. We also appreciate the resources provided by the LANL Institutional Computing (IC) program. R.A.M. acknowledges the Oak Ridge Leadership Computing Facility at the Oak Ridge National Laboratory, which is supported by the Office of Science of the U.S. Department of Energy under Contract No. DE-AC05-00OR22725.

-
- [1] I. Konovalov and Y. Stetsky, *Development status of metallic, dispersion and non-oxide advanced and alternative fuels for power and research reactors* (INTERNATIONAL ATOMIC ENERGY AGENCY, 2003).
- [2] D. Petti, D. Crawford, and N. Chauvin, Fuels for advanced nuclear energy systems, *MRS Bulletin* **34**, 40 (2009).
- [3] H. Matzke, *Science of advanced LMFBR fuels* (1986).
- [4] B. Frost, The carbides of uranium, *Journal of Nuclear Materials* **10**, 265 (1963).
- [5] G. Vasudevamurthy and A. T. Nelson, Uranium carbide properties for advanced fuel modeling—A review, *Journal of Nuclear Materials* **558**, 153145 (2022).
- [6] M. Freyss, First-principles study of uranium carbide: Accommodation of point defects and of helium, xenon, and oxygen impurities, *Physical Review B* **81**, 014101 (2010).
- [7] R. Ducher, R. Dubourg, M. Barrachin, and A. Pasturel, First-principles study of defect behavior in irradiated uranium monocarbide, *Physical Review B* **83**, 104107 (2011).
- [8] E. Bévilion, R. Ducher, M. Barrachin, and R. Dubourg, First-principles study of the stability of fission products in uranium monocarbide, *Journal of Nuclear Materials* **426**, 189 (2012).
- [9] E. Bévilion, R. Ducher, M. Barrachin, and R. Dubourg, Investigation of the diffusion of atomic fission products in UC by density functional calculations, *Journal of Nuclear Materials* **434**, 240 (2013).
- [10] H. Shi, P. Zhang, S.-S. Li, B. Sun, and B. Wang, Electronic structures and mechanical properties of uranium monocarbide from first-principles LDA+U and GGA+U calculations, *Physics Letters A* **373**, 3577 (2009).
- [11] U. D. Wdowik, P. Piekarczyk, D. Legut, and G. Jagło, Effect of spin-orbit and on-site coulomb interactions on the electronic structure and lattice dynamics of uranium monocarbide, *Physical Review B* **94**, 054303 (2016).
- [12] G. Y. Huang, G. Pastore, and B. D. Wirth, First-principles study of intrinsic point defects and Xe impurities in uranium monocarbide, *Journal of Applied Physics* **128**, 145102 (2020).
- [13] C. B. Basak, Classical molecular dynamics simulation of uranium monocarbide (UC), *Computational Materials Science* **40**, 562 (2007).

- [14] A. Chartier and L. V. Brutzel, Modeling of point defects and rare gas incorporation in uranium mono-carbide, [Nuclear Instruments and Methods in Physics Research Section B: Beam Interactions with Materials and Atoms](#) **255**, 146 (2007).
- [15] H. Chen, D. Yuan, H. Geng, W. Hu, and B. Huang, Development of a machine-learning interatomic potential for uranium under the moment tensor potential framework, [Computational Materials Science](#) **229**, 112376 (2023).
- [16] E. Stippell, L. Alzate-Vargas, K. N. Subedi, R. M. Tutchton, M. W. Cooper, S. Tretiak, T. Gibson, and R. A. Messerly, Building a DFT+U machine learning interatomic potential for uranium dioxide, [Artificial Intelligence Chemistry](#) **2**, 100042 (2024).
- [17] E. T. Dubois, J. Tranchida, J. Bouchet, and J. B. Maillet, Atomistic simulations of nuclear fuel UO_2 with machine learning interatomic potentials, [Physical Review Materials](#) **8**, 025402 (2024).
- [18] L. Alzate-Vargas, K. N. Subedi, N. Lubbers, M. W. D. Cooper, R. M. Tutchton, T. Gibson, and R. A. Messerly, [Toward machine learning interatomic potentials for modeling uranium mononitride](#) (2025), [arXiv:2411.14608 \[cond-mat.mtrl-sci\]](#).
- [19] N. Lubbers, J. S. Smith, and K. Barros, Hierarchical modeling of molecular energies using a deep neural network, [Journal of Chemical Physics](#) **148**, 241715 (2018).
- [20] M. Chigaev, J. S. Smith, S. Anaya, B. Nebgen, M. Bettencourt, K. Barros, and N. Lubbers, Lightweight and effective tensor sensitivity for atomistic neural networks, [Journal of Chemical Physics](#) **158**, 184108 (2023).
- [21] P. E. Blochl, Projector augmented-wave method, [Physical Review B](#) **50**, 17953 (1994).
- [22] G. Kresse and J. Furthmüller, Efficiency of ab-initio total energy calculations for metals and semiconductors using a plane-wave basis set, [Computational Materials Science](#) **6**, 15 (1996).
- [23] G. Kresse and D. Joubert, From ultrasoft pseudopotentials to the projector augmented-wave method, [Physical Review B](#) **59**, 1758 (1999).
- [24] J. P. Perdew, K. Burke, and M. Ernzerhof, Generalized gradient approximation made simple, [Physical Review Letters](#) **77**, 3865 (1996).
- [25] S. L. Dudarev, G. A. Botton, S. Y. Savrasov, C. J. Humphreys, and A. P. Sutton, Electron-energy-loss spectra and the structural stability of nickel oxide: An LSDA+U study, [Phys. Rev. B](#) **57**, 1505 (1998).

- [26] V. Wang, N. Xu, J.-C. Liu, G. Tang, and W.-T. Geng, VASPKIT: A user-friendly interface facilitating high-throughput computing and analysis using VASP code, *Computer Physics Communications* **267**, 108033 (2021).
- [27] A. Togo, First-principles phonon calculations with phonopy and phono3py, *J. Phys. Soc. Jpn.* **92**, 012001 (2023).
- [28] J. Jackman, T. Holden, W. Buyers, P. De V. Duplessis, O. Vogt, and J. Genossar, Systematic study of the lattice dynamics of the uranium rocksalt-structure compounds, *Physical Review B* **33**, 7144 – 7153 (1986).
- [29] L. J. Graham, H. Nadler, and R. Chang, Elastic constants of UC, *Journal of Applied Physics* **34**, 1572 (1963).
- [30] J. Routbort, Adiabatic elastic constants of uranium monocarbide, *Journal of Nuclear Materials* **40**, 17 (1971).
- [31] S. M. Butorin, S. Bauters, L. Amidani, A. Beck, A. Rossberg, S. Weiss, T. Vitova, K. O. Kvashnina, and O. Tougait, Effect of carbon content on electronic structure of uranium carbides, *Scientific Reports* **13**, 20434 (2023).
- [32] J. S. Smith, B. Nebgen, N. Lubbers, O. Isayev, and A. E. Roitberg, Less is more: Sampling chemical space with active learning, *The Journal of Chemical Physics* **148**, 241733 (2018).
- [33] J. S. Smith, B. Nebgen, N. Mathew, J. Chen, N. Lubbers, L. Burakovsky, S. Tretiak, H. A. Nam, T. Germann, S. Fensin, and K. Barros, Automated discovery of a robust interatomic potential for aluminum, *Nature Communications* **12**, 1257 (2021).
- [34] GitHub -lanl/hippynn at hippynn-0.0.3— github.com, <https://github.com/lanl/hippynn/>.
- [35] A. P. Thompson, H. M. Aktulga, R. Berger, D. S. Bolintineanu, W. M. Brown, P. S. Crozier, P. J. in 't Veld, A. Kohlmeyer, S. G. Moore, T. D. Nguyen, R. Shan, M. J. Stevens, J. Tranchida, C. Trott, and S. J. Plimpton, LAMMPS - a flexible simulation tool for particle-based materials modeling at the atomic, meso, and continuum scales, *Computer Physics Communications* **271**, 108171 (2022).
- [36] C. Utton, F. De Bruycker, K. Boboridis, R. Jardin, H. Noel, C. Guéneau, and D. Manara, Laser melting of uranium carbides, *Journal of Nuclear Materials* **385**, 443 (2009).
- [37] R. Méndez-Peñalosa and R. E. Taylor, Thermal expansion of uranium monocarbide, *Journal of the American Ceramic Society* **47**, 101 (1964).
- [38] H. Matzke, Point defects and transport properties in carbides, *Solid State Ionics* **12**, 25 (1984).

- [39] W. Schüle and P. Spindler, Properties of vacancies in uranium carbide, [Journal of Nuclear Materials](#) **32**, 20 (1969).
- [40] H. Matsui and H. Matzke, Quenched-in defects in UC and UCN, [Journal of Nuclear Materials](#) **89**, 41 (1980).
- [41] W. Chubb, R. Getz, and C. Townley, Diffusion in uranium monocarbide, [Journal of Nuclear Materials](#) **13**, 63 (1964).
- [42] H. M. Lee and L. Barbett, Diffusion of carbon and uranium in uranium carbide, [Journal of Nuclear Materials](#) **27**, 275 (1968).
- [43] R. A. Krakowski, Self-diffusion of carbon in uranium monocarbide, [Journal of Nuclear Materials](#) **32**, 120 (1969).
- [44] Y. Makino, K. Asahi, P. son, M. Miyake, and T. Sano, Self-diffusion of carbon in uranium monocarbide, [Journal of Nuclear Science and Technology](#) **9**, 569 (1972).
- [45] G. G. Bentle and J. Ervin, G., *Self-diffusion of uranium and carbon in uranium monocarbide*, Tech. Rep. (Atomics International, A Division of North American Rockwell Corporation, 1968) issued: August 30, 1968; Contract: AT(04-3)-701.

Supplementary Information for:

Atomistic modeling of uranium monocarbide with a machine learning interatomic potential.

We calculated the specific heat capacity at constant pressure, shown in Fig. S1a and bulk moduli, shown in Fig. S1b as a function of temperature.

Since MD calculations only capture the vibrational component of the heat capacity—excluding electronic (quantum) and magnetic contributions—there is a large discrepancy with the experimental-inferred heat capacity [1], particularly at low temperatures, where the quantum effects are stronger. However, the MLIP captures the increase in heat capacity at high temperatures, seen in UC, and correlated to the thermally activated point defects [2]. The bulk moduli calculated at zero-pressure, correctly predicts the inverse relation between bulk modulus and lattice expansion. The value at 300 K, agrees with the experimental data reported around 156–158 GPa.

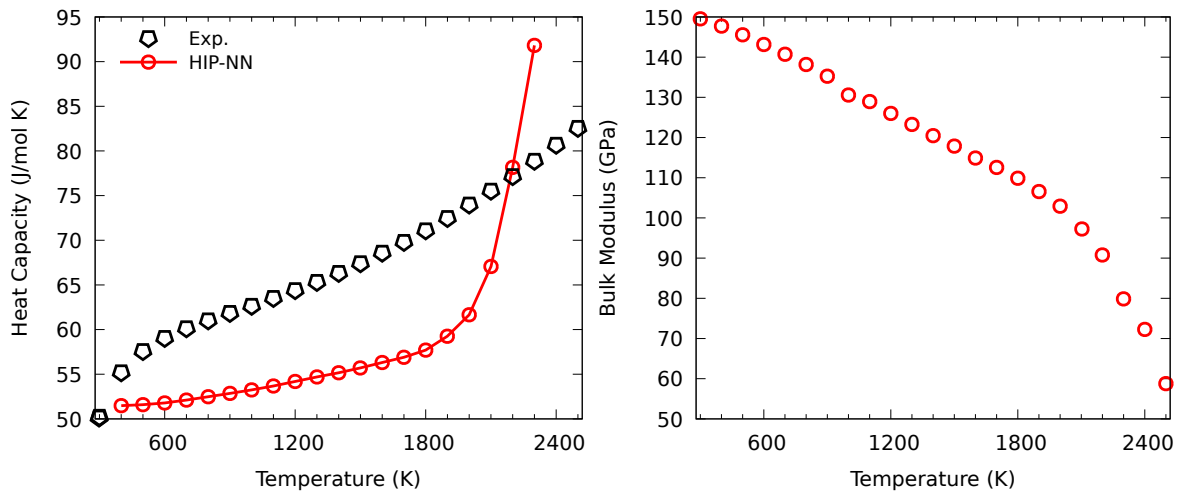


Figure S1: MLIP predicted thermophysical properties as function of temperature. Specific heat capacity with experimental data from Ref. [1] (left), and bulk moduli (right).

References

- [1] G. Vasudevamurthy and A. T. Nelson, Uranium carbide properties for advanced fuel modeling—A review, *Journal of Nuclear Materials* **558**, 153145 (2022).
- [2] M. Pavlov, et al., Measurement and interpretation of the thermo-physical properties of UO_2 at high temperatures: The viral effect of oxygen defects, *Acta Materialia* **139**, 138 (2017).